LUND UNIVERSITY

Collective and noncollective states in (120)Te

Nag, Somnath; Singh, A. K.; Wilson, A. N.; Rogers, J.; Huebel, H.; Buerger, A.; Chmel, S.; Ragnarsson, Ingemar; Sletten, G.; Herskind, B.; Carpenter, M. P.; Janssens, R. V. F.; Khoo, T. L.; Kondev, F. G.; Lauritsen, T.; Zhu, S.; Korichi, A.; Ha, Hoa; Fallon, P.; Macchiavelli, A. O.; Nyako, B. M.; Timar, J.; Juhasz, K.

Published in:
Physical Review C (Nuclear Physics)

DOI:
10.1103/PhysRevC.85.014310

2012

Link to publication

Citation for published version (APA):
Nag, S., Singh, A. K., Wilson, A. N., Rogers, J., Huebel, H., Buerger, A., Chmel, S., Ragnarsson, I., Sletten, G., Herskind, B., Carpenter, M. P., Janssens, R. V. F., Khoo, T. L., Kondev, F. G., Lauritsen, T., Zhu, S., Korichi, A., Ha, H., Fallon, P., ... Juhasz, K. (2012). Collective and noncollective states in (120)Te. *Physical Review C (Nuclear Physics)*, *85*(1), [014310]. https://doi.org/10.1103/PhysRevC.85.014310

Total number of authors:
23

General rights
Unless other specific re-use rights are stated the following general rights apply:
Copyright and moral rights for the publications made accessible in the public portal are retained by the authors and/or other copyright owners and it is a condition of accessing publications that users recognise and abide by the legal requirements associated with these rights.
• Users may download and print one copy of any publication from the public portal for the purpose of private study or research.
• You may not further distribute the material or use it for any profit-making activity or commercial gain
• You may freely distribute the URL identifying the publication in the public portal

Read more about Creative commons licenses: https://creativecommons.org/licenses/

Take down policy
If you believe that this document breaches copyright please contact us providing details, and we will remove access to the work immediately and investigate your claim.

LUND UNIVERSITY

PO Box 117
221 00 Lund
+46 46-222 00 00

Download date: 08. Oct. 2022

PHYSICAL REVIEW C **85**, 014310 (2012)

Collective and noncollective states in ^{120}Te

Somnath Nag and A. K. Singh
Department of Physics and Meteorology, Indian Institute of Technology Kharagpur, Kharagpur, IN-721302, India

A. N. Wilson and J. Rogers
Research School of Physics and Engineering, The Australian National University, Canberra, ACT 0200 Australia

H. Hübel, A. Bürger, and S. Chmel
Helmholtz-Institut für Strahlen- und Kernphysik, Universität Bonn, Nussallee 14-16, D-53115 Bonn, Germany

I. Ragnarsson
Division of Mathematical Physics, LTH, Lund University, Box 118, S-22100 Lund, Sweden

G. Sletten and B. Herskind
Niels Bohr Institute, Blegdamsvej 17, DK-2100 Copenhagen, Denmark

M. P. Carpenter, R. V. F. Janssens, T. L. Khoo, F. G. Kondev, T. Lauritsen, and S. Zhu
Physics Division, Argonne National Laboratory, Argonne, Illinois 60439, USA

A. Korichi and Hoa Ha
CSNSM-IN2P3, F-91405 Orsay Campus, France

P. Fallon and A. O. Macchiavelli
Nuclear Science Division, Lawrence Berkeley National Laboratory, Berkeley, California 94720, USA

B. M. Nyakó and J. Timár
Institute of Nuclear Research of the Hungarian Academy of Sciences, H-4001 Debrecen, Hungary

K. Juhász
Department of Information Technology, University of Debrecen, H-4032, Hungary

(Received 2 November 2011; published 13 January 2012)

High-spin states in ^{120}Te were populated in the reaction ^{80}Se(^{48}Ca, $\alpha 4n$)^{120}Te at a beam energy of 207 MeV and γ-ray coincidences were measured using the Gammasphere spectrometer. The previously known level scheme is extended to higher spin and new interband transitions and side-feeding branches are established. Five highly deformed rotational bands, extending up to almost $I = 50$, are observed for the first time. The bands are compared with similar structures found recently in neighboring nuclei. The experimental results are interpreted within the framework of the cranked Nilsson-Strutinsky model. Configuration assignments to several terminating states and to the high-spin bands are discussed.

DOI: 10.1103/PhysRevC.85.014310 PACS number(s): 23.20.Lv, 23.20.En, 27.60.+j, 21.60.Ev

I. INTRODUCTION

Nuclei near the $Z = 50$ proton shell closure are known to exhibit shape coexistence [1], which has been investigated in detail in many neutron deficient isotopes of Sn [2], Sb [3–5], and Te [6,7]. The available small number of valence particles or holes can break the spherical symmetry and, thus, drive the nucleus towards (small) deformation. As a result, collective structures compete energetically with the oblate states dominated by the contribution from single-particle excitations [8].

Shape changes as a function of spin are observed due to the opposite shape-driving tendencies of protons and neutrons, especially those in high-j orbitals. In the mass-120 region, protons fill low-Ω $h_{11/2}$ orbitals, which favor a prolate shape, while neutrons occupy medium-to-high-Ω $h_{11/2}$ orbitals, which drive the nuclei towards an oblate shape.

Progressive alignment of neutrons and protons may result in a shape change from a prolate deformation at low spin to an oblate shape at higher spin via intermediate states associated with a triaxial shape. The orbitals lying close to the Fermi surface are the dominant contributors [9]. With a limited number of particles in the valence space, the alignment of all these particles to the maximum possible spin leads to oblate states with $\varepsilon_2 \simeq 0.15$ for nuclei in the mass-120 region. Total Routhian surface (TRS) and cranked Nilsson-Strutinsky (CNS) calculations have been used to investigate these fully aligned states [10–12].

 ©2012 American Physical Society

Furthermore, collective bands based on particle-hole excitations across the $Z = 50$ shell gap from the energetically upsloping $g_{9/2}$ into downsloping mixed $g_{7/2}d_{5/2}$ or $h_{11/2}$ orbitals have been observed. These excitations are favored at prolate deformation with $\varepsilon_2 \simeq 0.2$ and $\gamma \simeq 0^\circ$ [2,6,13–15]. The sequences terminate when the spins of all the valence nucleons are aligned with the symmetry axis. If this alignment occurs gradually and the moments of inertia decrease smoothly with increasing spin, this phenomenon is referred to as smooth band termination [3,16,17].

Recently, highly deformed high-spin bands have been discovered in nuclei around $N = 70$ in ^{125}I [18], ^{125}Xe [19], ^{126}Xe [20], and ^{124}Ba [21]. They generally start around $I \simeq 25$ and continue up to $I \simeq 50$–60. Their configurations involve neutron excitations into $i_{13/2}$ orbitals across the $N = 82$ shell gap and particle-hole excitations from the $g_{9/2}$ orbital across the $Z = 50$ shell closure. Transition quadrupole moments ranging from 4.3 to 5.9 b have been estimated for these bands in ^{125}Xe [19] and ^{126}Xe [20], which translate into deformation parameters ε_2 from 0.27 to 0.36. In somewhat heavier nuclei, around $A = 130$, superdeformed (SD) shapes with deformation parameters of $\varepsilon_2 \simeq 0.4$ have been observed [22,23].

The present work reports on a study of ^{120}Te with the aim to locate the noncollective fully aligned states in this nucleus and to search for highly deformed high-spin bands, similar to those observed in the neighboring heavier nuclei.

The experimental setup and the off-line analysis are briefly described in Sec. II. Experimental results and the level scheme are presented in Sec. III. In Sec. IV the results are discussed within the framework of the CNS model, followed by a brief summary in Sec. V.

II. EXPERIMENTAL DETAILS AND DATA ANALYSIS

High-spin states in ^{120}Te were populated in the heavy-ion reaction ^{80}Se(^{48}Ca, $\alpha 4n$)^{120}Te. The ^{48}Ca beam, with an energy of 207 MeV and an intensity of 4 pnA, was provided by the ATLAS accelerator at Argonne National Laboratory. The target consisted of a ^{80}Se layer with a thickness of 600 μg/cm^2 evaporated onto a 300 μg/cm^2 Au backing. The ^{80}Se was protected by 40 μg/cm^2 Au. The Au backing faced the beam. For heat dissipation, the target was mounted on four quadrants of a rotating wheel and the incident beam was slightly defocused and wobbled. The dominant reaction channels were $4n$, $5n$, $p4n$, and $\alpha 4n$ leading to ^{124}Xe, ^{123}Xe, ^{123}I, and ^{120}Te residual nuclei, respectively.

Graded absorbers consisting of a Ta-Cd-Cu combination were used to shield the detectors from low-energy x rays. Gamma-ray coincidences were measured with the Gammasphere spectrometer [24], which consisted of 101 Compton-suppressed Ge detectors at the time of the experiment. A total of 2.7×10^9 γ-ray coincidence events were recorded with Ge-detector fold $\geqslant 4$ in ten days of beam time.

In the off-line analysis, the gain-matched and calibrated data were sorted into three- and four-dimensional arrays (cubes and hypercubes, respectively) using the RADWARE software package [25]. Relative γ-ray intensities were measured and normalized to the 614-keV $6^+ \rightarrow 4^+$ transition. In order to determine the multipolarities of the transitions, the following two matrices were sorted. The first one included the events detected in detectors at forward ($\simeq 35^\circ$) and backward ($\simeq 145^\circ$) angles on one axis (fb) and those detected in all detectors on the other axis (all), whereas the second matrix consisted of events registered in detectors near 90° on one axis (90) and those in all detectors on the second axis (all). Angular distribution ratios, R_θ, were determined by placing coincidence gates in these matrices on the axes with events detected in all detectors. The intensity ratios

$$R_\theta = \frac{I(\gamma 1_{fb}, \gamma 2_{\mathrm{all}})}{I(\gamma 1_{90}, \gamma 2_{\mathrm{all}})}$$

for stretched dipole and stretched quadrupole transitions lie around 0.6 and 1.2, respectively.

III. RESULTS AND LEVEL SCHEME

The level scheme of ^{120}Te, based on the present results and on previous work [26,27], is shown in Fig 1. Gamma-ray transition energies, intensities, angular distribution ratios, deduced multipolarities, and spin-parity assignments are listed in Table I. For the spin and parity assignments it was assumed that stretched quadrupole transitions are of $E2$ character (rather than $M2$ transitions, which are strongly hindered). In some cases, the presence of crossover transitions or the feeding pattern to other levels helped to fix spins and parities. Spin and parity assignments to states in the lower part of the level scheme were adopted from previous work [26,27].

A. Medium-spin states

Excited states in ^{120}Te were observed in previous investigations up to $I^\pi = 13^-$ [26] and 16^+ [27], respectively. In the present work, higher-spin states, new side-feeding branches, and crossover transitions were added. Two examples of the γ-ray coincidence spectra from the low- to medium-spin range are displayed in Fig. 2.

A cascade of three stretched quadrupole, presumably $E2$, transitions (sequence c in Fig. 1) was placed on top of the 13^- state. The highest-energy level in this sequence, the $I^\pi = 19^-$ state at 7279 keV, decays via the 410-keV unstretched dipole, presumably $M1$, transition to the 19^- level at 6869 keV and via two cascades down to the 16^+ state at 5343 keV of sequence a.

Two cascades of transitions with energies of 1197 and 448 keV and of 226 and 893 keV, respectively, have been placed on top of the new 18^+ state at 6643 keV. The angular distributions of the 1197- and 448-keV transitions are compatible with stretched quadrupoles, presumably of $E2$ multipolarity, which fixes $I^\pi = 20^+$ and 22^+ for the 7840- and 8289-keV states, respectively. The sequence of transitions labeled f in Fig. 1 feeds into the 8289-keV level. The ordering of its members could be established only for the 852- and 872-keV transitions from their measured intensities.

The $E2$ transitions with energies of 483, 950, and 505 keV have been placed on top of the 7279-keV

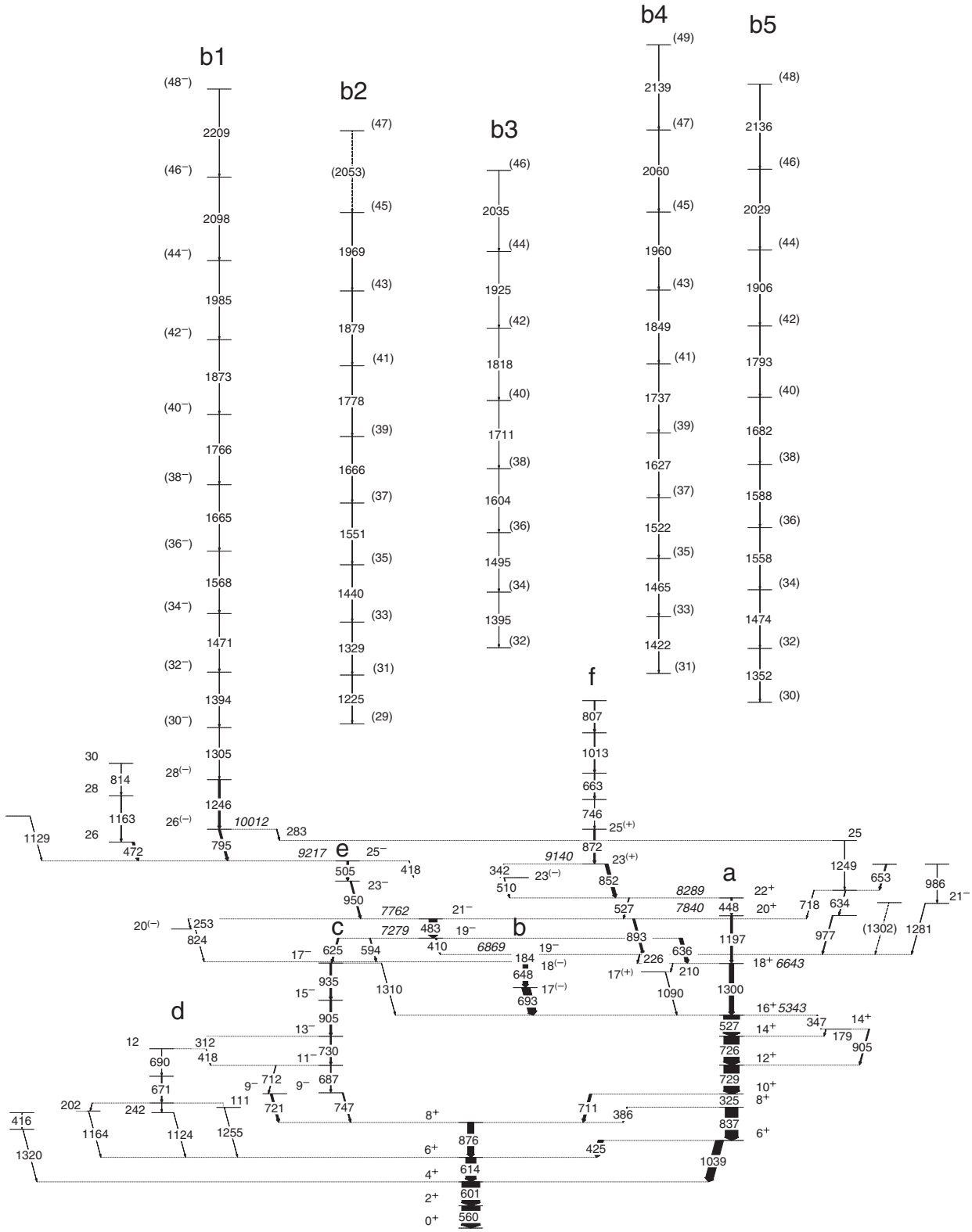

FIG. 1. Level scheme of ^{120}Te based on present results and on previous work [26,27]. The width of the arrows corresponds to the γ-ray intensities.

$I^{\pi} = 19^{-}$ state. Thus, $I^{\pi} = 25^{-}$ is assigned to the new level at 9217 keV. The 7762-keV $I^{\pi} = 21^{-}$ state within this sequence decays to the $I^{\pi} = 19^{-}$ level at 6869 keV (see above) via the 893-keV $E2$ transition. Transitions populating the $I^{\pi} = 25^{-}$ state appear also in coincidence with the 852-keV γ ray, suggesting the existence of an unobserved low-energy transition between the 9217- and 9140-keV levels.

TABLE I. Gamma-ray energies, intensities, angular distribution ratios, spin assignments, level energies, and γ-ray multipolarities for transitions placed in ^{120}Te.

Energy E_γ^a [keV]	Intensity I_γ	Intensity ratio R_θ	$I_i^\pi \rightarrow I_f^\pi$	Level energy E_i [keV]	Assigned multipolarity
111.0	7(2)	–	–	3141.0	–
179.1	9(2)	–	$14^+ \rightarrow 14^+$	4995.6	–
183.8	161(16)	0.46(7)	$19^- \rightarrow 18^{(-)}$	6868.7	$M1$ or $E1$
202.0	8(1)	–	–	3141.0	–
210.3	11(2)	0.54(8)	$18^+ \rightarrow 17^{(+)}$	6643.0	$M1$ or $E1$
225.7	22(2)	0.67(11)	$19^- \rightarrow 18^+$	6868.7	$E1$
242.0	7(2)	–	–	3141.0	–
252.6	8(2)	–	$21^- \rightarrow 20^{(-)}$	7761.7	$M1$ or $E1$
283.0	26(3)	0.66(10)	$26^{(-)} \rightarrow 25$	10012.0	$M1$ or $E1$
311.6	17(2)	0.66(20)	$13^- \rightarrow 12$	4814.0	$M1$ or $E1$
325.0	584(29)	1.51(11)	$10^+ \rightarrow 8^+$	3361.9	$E2$
341.8	41(2)	0.70(5)	$23^{(+)} \rightarrow 23^{(-)}$	9140.3	$M1$ or $E1$
347.5	25(3)	1.38(15)	$16^+ \rightarrow 14^+$	5343.1	$E2$
386.3	29(2)	1.46(11)	$8^+ \rightarrow 8^+$	3036.9	$M1$
410.2	46(4)	1.55(33)	$19^- \rightarrow 19^-$	7278.9	$M1$
416.0[b]	–	–	–	2897.0	–
418.1[b]	13(4)	–	$12 \rightarrow 11^-$	4502.4	$M1$ or $E1$
418.5[b]	17(5)	–	$25^- \rightarrow 23^-$	9217.0	$E2$
424.9	260(15)	1.31(9)	$6^+ \rightarrow 6^+$	2199.7	$M1$
448.1	72(5)	1.58(11)	$22^+ \rightarrow 20^+$	8288.6	$E2$
472.0	83(7)	0.66(9)	$26 \rightarrow 25^-$	9689.0	$M1$ or $E1$
482.8	396(20)	1.64(11)	$21^- \rightarrow 19^-$	7761.7	$E2$
505.4	85(6)	1.33(9)	$25^- \rightarrow 23^-$	9217.0	$E2$
509.9	30(2)	0.66(3)	$23^{(-)} \rightarrow 22^+$	8798.5	$M1$ or $E1$
526.6	790(40)	1.25(9)	$16^+ \rightarrow 14^+$	5343.1	$E2$
526.9	41(10)	0.81(6)	$22^+ \rightarrow 21^-$	8288.6	$E1$
560.0	–	–	$2^+ \rightarrow 0^+$	560.0	$E2$
594.0	48(2)	0.48(6)	$19^- \rightarrow 18^{(-)}$	7278.9	$M1$ or $E1$
600.6	–	–	$4^+ \rightarrow 2^+$	1160.6	$E2$
614.2	500[e]	1.62(11)	$6^+ \rightarrow 4^+$	1774.8	$E2$
625.4	77(4)	1.58(16)	$19^- \rightarrow 17^-$	7278.9	$E2$
634.3[b]	30(4)	–	–	8480.0	–
635.9	171(9)	0.59(4)	$19^- \rightarrow 18^+$	7278.9	$E1$
648.4	240(12)	0.47(3)	$18^{(-)} \rightarrow 17^{(-)}$	6684.9	$M1$ or $E1$
653.0[b]	25(3)	–	–	9133.0	–
663.0	53(10)	1.12(22)	–	11421.3	$E2$
671.0	38(6)	0.80(6)	–	3812.0	$M1/E2$
686.9	36(8)	1.30(13)	$11^- \rightarrow 9^-$	4084.3	$E2$
690.4[b]	–	–	$12 \rightarrow -$	4502.4	–
693.4	399(20)	0.79(6)	$17^{(-)} \rightarrow 16^+$	6036.5	$M1$ or $E1$
711.3	119(6)	1.53(10)	$10^+ \rightarrow 8^+$	3361.9	$E2$
712.4	36(5)	1.41(10)	$11^- \rightarrow 9^-$	4084.3	$E2$
718.3[b]	–	–	$- \rightarrow 21^-$	8480.0	–
721.2	44(2)	0.59(5)	$9^- \rightarrow 8^+$	3371.8	$E1$
726.0[c]	1532(80)	1.50(12)	$14^+ \rightarrow 12^+$	4816.5	$E2$
728.8[c]			$12^+ \rightarrow 10^+$	4090.7	$E2$
729.7	71(6)	1.44(10)	$13^- \rightarrow 11^-$	4814.0	$E2$
746.0	56(4)	0.95(19)	–	10758.3	$M1/E2$
746.8[b]	58(5)	–	$9^- \rightarrow 8^+$	3397.4	$E1$
795.0	95(5)	0.39(6)	$26^{(-)} \rightarrow 25^-$	10012.0	$M1/E2$
807.0	44(7)	1.23(25)	–	13241.3	$E2$
813.5	20(6)	1.48(30)	$30 \rightarrow 28$	11665.5	$E2$
824.2	27(3)	1.12(15)	$20^{(-)} \rightarrow 18^{(-)}$	7509.1	$E2$
837.2	629(31)	1.37(10)	$8^+ \rightarrow 6^+$	3036.9	$E2$
851.7	155(9)	0.45(13)	$23^{(+)} \rightarrow 22^+$	9140.3	$M1$ or $E1$

TABLE I. (*Continued.*)

Energy E_γ^a [keV]	Intensity I_γ	Intensity ratio R_θ	$I_i^\pi \rightarrow I_f^\pi$	Level energy E_i [keV]	Assigned multipolarity
872.0	85(5)	1.32(10)	$25 \rightarrow 23^{(+)}$	10012.3	$E2$
875.8	309(15)	1.56(11)	$8^+ \rightarrow 6^+$	2650.6	$E2$
893.0	107(5)	1.62(12)	$21^- \rightarrow 19^-$	7761.7	$E2$
904.6	80(4)	1.35(7)	$15^- \rightarrow 13^-$	5718.6	$E2$
904.9	49(7)	1.61(15)	$14^+ \rightarrow 12^+$	4995.6	$E2$
934.9	62(5)	1.50(15)	$17^- \rightarrow 15^-$	6653.5	$E2$
949.9	88(8)	1.52(11)	$23^- \rightarrow 21^-$	8711.6	$E2$
977.0[b]	46(2)	–	$- \rightarrow 19^-$	7845.7	–
985.9[b]	17(5)	–	–	9135.6	–
1013.0	45(12)	0.91(18)	–	12434.3	$M1/E2$
1039.1	390(40)	1.36(19)	$6^+ \rightarrow 4^+$	2199.7	$E2$
1089.6	25(1)	0.32(2)	$17^{(+)} \rightarrow 16^+$	6432.7	$M1$ or $E1$
1124.2	14(3)	–	$- \rightarrow 6^+$	2899.0	–
1129.0	22(5)	–	$- \rightarrow 25^-$	10346.0	–
1163.0	42(3)	1.44(20)	$28 \rightarrow 26$	10852.0	$E2$
1164.2[b]	–	–	–	2939.0	–
1197.5	106(11)	1.61(22)	$20^+ \rightarrow 18^+$	7840.5	$E2$
1249.0[b]	–	–	$25 \rightarrow -$	9729.0	–
1255.0[b]	–	–	–	3030.0	–
1281.0	22(5)	1.80(.3)	$21^- \rightarrow 19^-$	8149.7	$E2$
1299.9	360(37)	1.19(17)	$18^+ \rightarrow 16^+$	6643.0	$E2$
1310.0[b]	–	–	$17^- \rightarrow 16^+$	6653.5	$E1$
1320.4[b]	–	–	$- \rightarrow 4^+$	2481.0	–
Band b1					
1246[d]	125(13)	1.53(16)	$28^{(-)} \rightarrow 26^{(-)}$	11258	$E2$
1305[b]	–	–	$(30^-) \rightarrow 28^{(-)}$	12563	$(E2)$
1394	10[e]	–	$(32^-) \rightarrow (30^-)$	13957	$(E2)$
1471	13(5)	–	$(34^-) \rightarrow (32^-)$	15428	$(E2)$
1568	15(4)	–	$(36^-) \rightarrow (34^-)$	16996	$(E2)$
1665	11(5)	–	$(38^-) \rightarrow (36^-)$	18661	$(E2)$
1766	10(4)	–	$(40^-) \rightarrow (38^-)$	20427	$(E2)$
1873	10(3)	–	$(42^-) \rightarrow (40^-)$	22300	$(E2)$
1985	9 (3)	–	$(44^-) \rightarrow (42^-)$	24285	$(E2)$
2098	< 5	–	$(46^-) \rightarrow (44^-)$	26383	$(E2)$
2209	< 5	–	$(48^-) \rightarrow (46^-)$	28592	$(E2)$
Band b2					
1225	10[e]	–	$(31) \rightarrow (29)$	Y + 13884	$(E2)$
1329	17(5)	–	$(33) \rightarrow (31)$	Y + 15213	$(E2)$
1440	12(3)	–	$(35) \rightarrow (33)$	Y + 16653	$(E2)$
1551	11(4)	–	$(37) \rightarrow (35)$	Y + 18204	$(E2)$
1668	9(3)	–	$(39) \rightarrow (37)$	Y + 19872	$(E2)$
1778	7(2)	–	$(41) \rightarrow (39)$	Y + 21650	$(E2)$
1879	< 5	–	$(43) \rightarrow (41)$	Y + 23529	$(E2)$
1969	< 5	–	$(45) \rightarrow (43)$	Y + 25498	$(E2)$
2053	< 5	–	$(47) \rightarrow (45)$	Y + 27551	$(E2)$
Band b3					
1395	10[e]	–	$(34) \rightarrow (32)$	Z + 15965	$(E2)$
1495	12(4)	–	$(36) \rightarrow (34)$	Z + 17460	$(E2)$
1604	14(4)	–	$(38) \rightarrow (36)$	Z + 19064	$(E2)$
1711	15(4)	–	$(40) \rightarrow (38)$	Z + 20775	$(E2)$
1818	8(3)	–	$(42) \rightarrow (40)$	Z + 22593	$(E2)$
1925	< 5	–	$(44) \rightarrow (42)$	Z + 24518	$(E2)$
2035	< 5	–	$(46) \rightarrow (44)$	Z + 26553	$(E2)$

TABLE I. (*Continued.*)

Energy E_γ^a [keV]	Intensity I_γ	Intensity ratio R_θ	$I_i^\pi \rightarrow I_f^\pi$	Level energy E_i [keV]	Assigned multipolarity
Band b4					
1422	10[e]	–	(33) → (31)	V + 15346	($E2$)
1465	6(2)	–	(35) → (33)	V + 16811	($E2$)
1522	11(4)	–	(37) → (35)	V + 18333	($E2$)
1627	11(4)	–	(39) → (37)	V + 19960	($E2$)
1737	10(3)	–	(41) → (39)	V + 21697	($E2$)
1849	9(3)	–	(43) → (41)	V + 23546	($E2$)
1960	6(2)	–	(45) → (43)	V + 25506	($E2$)
2060	< 5	–	(47) → (45)	V + 27566	($E2$)
2139	< 5	–	(49) → (47)	V + 29705	($E2$)
Band b5					
1352	10[e]	–	(32) → (30)	W + 14552	($E2$)
1474	6(2)	–	(34) → (32)	W + 16026	($E2$)
1558	14(3)	–	(36) → (34)	W + 17582	($E2$)
1588	8(3)	–	(38) → (36)	W + 19170	($E2$)
1682	10(3)	–	(40) → (38)	W + 20852	($E2$)
1793	7(2)	–	(42) → (40)	W + 22645	($E2$)
1906	< 5	–	(44) → (42)	W + 24551	($E2$)
2029	< 5	–	(46) → (44)	W + 26580	($E2$)
2136	< 5	–	(48) → (46)	W + 28716	($E2$)

[a]Uncertainties lie between 0.2 and 0.6 keV depending on intensity. For bands b1 to b5 the uncertainties may vary up to 2 keV.
[b]Measurement of I_γ and/or R_θ not possible due to presence of a transition with overlapping energy.
[c]Combined intensity and average intensity ratio R_θ for the 726.0- and 728.8-keV transitions.
[d]The intensity of the 1246.0-keV γ transition is high due to the presence of a γ ray with an energy of 1249.0 keV.
[e]Intensities are normalised to this transition.

A relatively intense dipole transition of 795 keV feeds the 25^- state at 9217 keV. Its angular distribution ratio, $R_\theta = 0.39(6)$, is smaller than expected for a pure stretched dipole. This suggests that it is a mixed $M1/E2$ transition and, therefore, negative parity was tentatively assigned to the $I = 26$ level at 10012 keV. It is the band head of the new high-spin band b1 (see following subsection) and decays also to the 19^- state at 6869 keV via the cascade of transitions with 283, 1249, 634, and 977 keV.

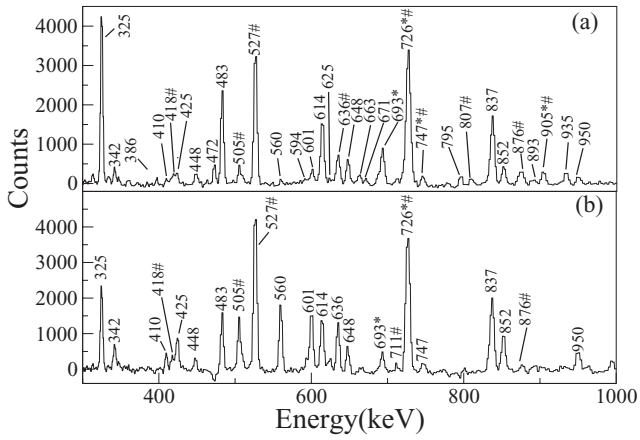

FIG. 2. Summed triple-gated γ-ray coincidence spectra from the low- and medium-energy part of the level scheme. Transitions marked by hash marks are unresolved doublets. (a) Spectrum created with gates on the 425-, 560-, 601-, 625-, and 1039-keV transitions. Transitions marked by asterisks belong to branch c or d and its connection with the low-lying yrast states. (b) Spectrum obtained with a gate on the 795-keV transition depopulating band b1 and with double gates on any transition from a list of energies of 325, 425, 483, 560, 601, 693, and 1039 keV.

B. High-spin bands

Five regular rotational bands, labeled b1 to b5 in Fig. 1, have been observed for the first time in ^{120}Te. In Figs. 3–5 summed triple-gated γ-ray coincidence spectra of these high-spin bands are displayed. Linking transitions to lower-energy levels could only be established for band b1. This band consists of eleven transitions and collects the highest intensity among the five bands. Its intensity lies around 8% of the population, whereas that of the other bands varies between 3 and 5%. The 1246-keV γ ray exhibits an angular distribution of a stretched quadrupole ($E2$) transition. Therefore, spins of 26 and 28, respectively, and negative parity were assigned to the two lowest levels of b1. No angular distribution ratios could be determined for the transitions between the higher-spin states within the band. However, because of the regularity of the band, $E2$ multipolarity was assumed for these γ rays.

The transitions linking bands b2 to b5 to lower-lying levels could not be established. However, it was observed that b2 decays through the 795-keV transition into branch e. Therefore, $I = 29$ was tentatively assigned to its band head.

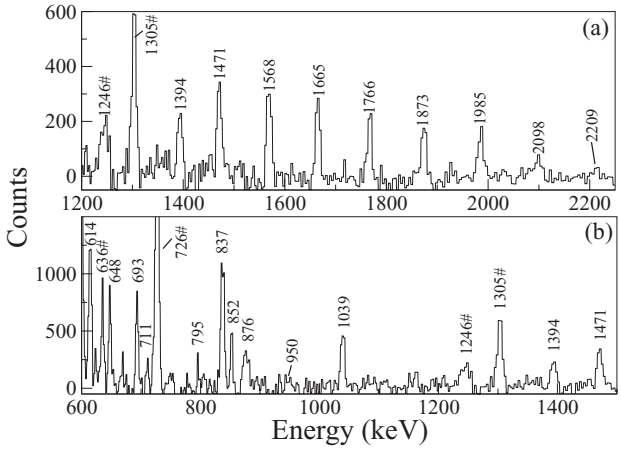

FIG. 3. Summed triple-gated γ-ray coincidence spectrum of band b1 created with a single gate from a list of transitions from the lower part of the level scheme with energies of 325, 425, 483, 560, 601, 693, and 1039 keV and with double gates on all transitions of b1 (except on 1305 keV). Hash-marked peaks are unresolved doublets.

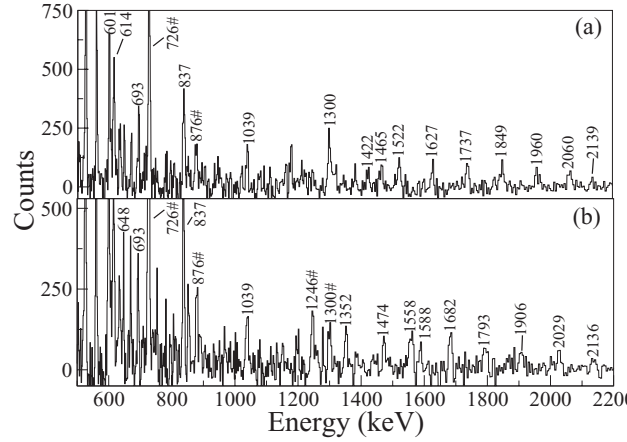

FIG. 5. Summed triple-gated γ-ray coincidence spectra for bands b4 (a) and b5 (b). The spectra were created with a list of transitions from the lower-spin states (energies given in Fig. 2) and with double gates on all transitions of b4 and b5, respectively. Hash-marked peaks are unresolved doublets.

Band b3 decays through branch f and bands b4 and b5 decay into the lower levels of b1. Thus, the spin range for their band heads is $I = 30$–33.

The tentatively assigned spins, as given in Fig. 1, are plotted as a function of γ-ray transition energy in Fig. 6. With these assignments, the spin values for the unconnected bands are 1–2 $\hbar$ larger at a fixed frequency than those of b1 where the spins are known.

IV. DISCUSSION

The low-spin states of ^{120}Te, up to $I^{\pi} = 8^{+}$, exhibit a vibrational structure. The energy ratios $E(4^{+})/E(2^{+}) = 2.07$ and $E(6^{+})/E(4^{+}) = 1.53$ lie close to the values for a perfect vibrator. The higher-spin states are characterized by quasiparticle excitations; and the opposite shape-driving effects of low-Ω $h_{11/2}$ protons and high-Ω $h_{11/2}$ neutrons lead to a variety of structures with different shapes. The high-spin region of the level scheme is dominated by regular bands with high collectivity.

The low-energy part of the level scheme was investigated previously [26,27]. Therefore, in the following, only the new medium-spin structures and the five high-spin rotational bands are discussed. Configurations are suggested by comparing the observed properties with the results of CNS calculations.

Within the framework of the CNS approach [17,28–31], pairing is neglected. Therefore, the results are relevant mainly for high-spin excitations, but also in the intermediate-spin regime ($I > 15$) reasonable agreement with experimental results was obtained previously for other nuclei [32,33]. A unique feature of the CNS formalism is the possibility to fix configurations in more detail than in any other similar

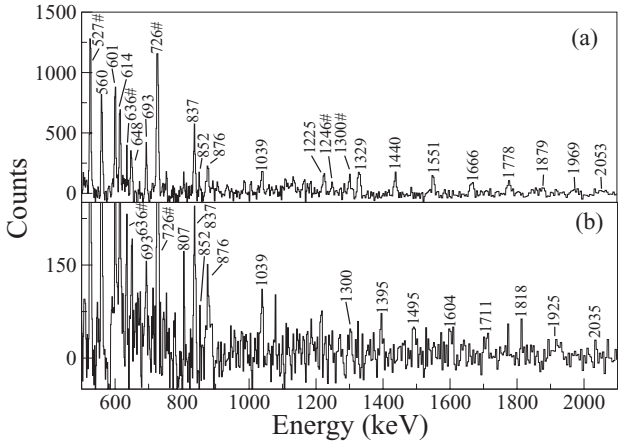

FIG. 4. Summed triple-gated γ-ray coincidence spectra for bands b2 (a) and b3 (b). The spectra were created with a list of transitions from the lower-spin states (energies given in Fig. 2) and with double gates on all transitions of b2 up to 1879 keV and all transitions of b3 up to 2035 keV, respectively. Hash-marked peaks are unresolved doublets.

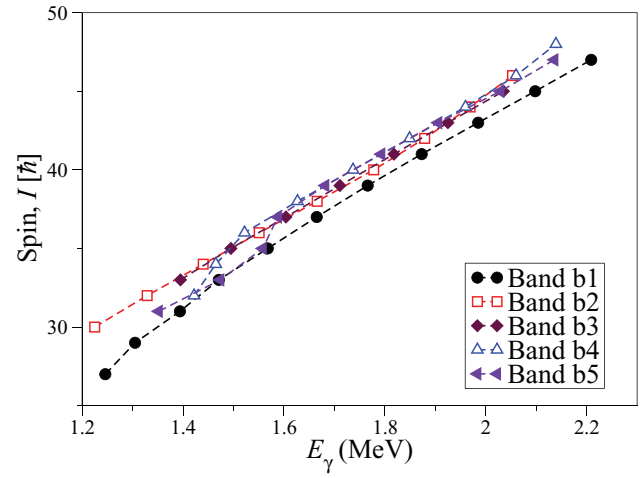

FIG. 6. (Color online) Spin as a function of E_{γ} for the five new high-spin bands in ^{120}Te. The spin values for the unconnected bands are tentative.

approach because the eigenfunctions of the rotating harmonic oscillator [34] are used as basis states in the single-particle diagonalization. The matrix elements which couple the principle $N_{\rm rot}$ shells in this basis are small. Therefore, they can be neglected to good approximation and $N_{\rm rot}$ may be treated as a preserved quantum number [28]. Then, within each $N_{\rm rot}$ shell, a further division into orbitals having their main amplitude in the high-j intruder shell and in the other low-j shells is possible [16]. With this labeling of the orbitals, it is straightforward to fix configurations by the number of particles in groups characterized by (i) $N_{\rm rot}$, (ii) low-j or high-j shells, and (iii) signature $\alpha = 1/2$ and $\alpha = -1/2$. For a general understanding of the configurations, it is instructive to specify them according to the number of valence particles in different j shells or groups of j shells. For ^{120}Te it is convenient to use $^{114}_{50}$Sn$_{64}$ as a core and use the labels

$$[p_1 p_2, n_1(n_2 n_3)],$$

where p_1 and p_2 are the numbers of proton holes in $g_{9/2}$ and protons in $h_{11/2}$ orbitals, respectively, whereas the number of neutrons occupying $h_{11/2}$, $(h_{9/2} f_{7/2})$, and $i_{13/2}$ orbitals is represented by n_1, n_2, and n_3, respectively. The number of particles in the other valence shells; i.e., the low-j $N = 4$ orbitals for protons and neutrons, is then determined to obtain the correct total number of particles, $Z = 52$ and $N = 68$. It should be noted that this labeling is only approximate and essentially all couplings between the j-shells are accounted for as outlined above. Especially, no distinction is made between valence particles and the core.

In the present calculation the parameters κ and μ, derived for the $A = 110$ region [35], have been applied. The Lublin-Strasbourg drop (LSD) model [36] is used for the static liquid-drop energy. The rigid-body moments of inertia are calculated with a radius parameter of $r_0 = 1.16$ fm and a diffuseness of $a = 0.6$ fm [31]. An energy scale based on mass excess is applied so that calculated energies can be directly compared with experimentally observed energies. Furthermore, energies of high-spin states in different nuclei can be compared in a similar way as the masses of the ground states. The calculations minimize the energies for different configurations and for different spins with respect to the deformation parameters ε_2, ε_4, and γ. Here, ε_2 and γ are the standard quadrupole deformation parameters describing elongation and axial asymmetry, respectively, while the hexadecapole deformation, described by ε_4, is defined in such a way that the axial symmetry is preserved for oblate ($\gamma = \pm 60^\circ$) and prolate ($\gamma = 0^\circ, -120^\circ$) shape [28,37].

A. Medium-spin states

Calculated single-particle energies for protons and neutrons are plotted as a function of the spin-projection quantum number in Fig. 7. The tilted Fermi surface method [38,39] can be used to find the optimal configurations. Several straight lines are drawn in Fig. 7, corresponding to favored excited states outside the $^{114}_{50}$Sn$_{64}$ core. They are

$$\nu(h_{11/2})^4; I^\pi_{\rm max} = (8^+), 10^+, 16^+, \quad \nu\left(h^3_{11/2}, d_{3/2}\right); I^\pi_{\rm max} = 15^-$$

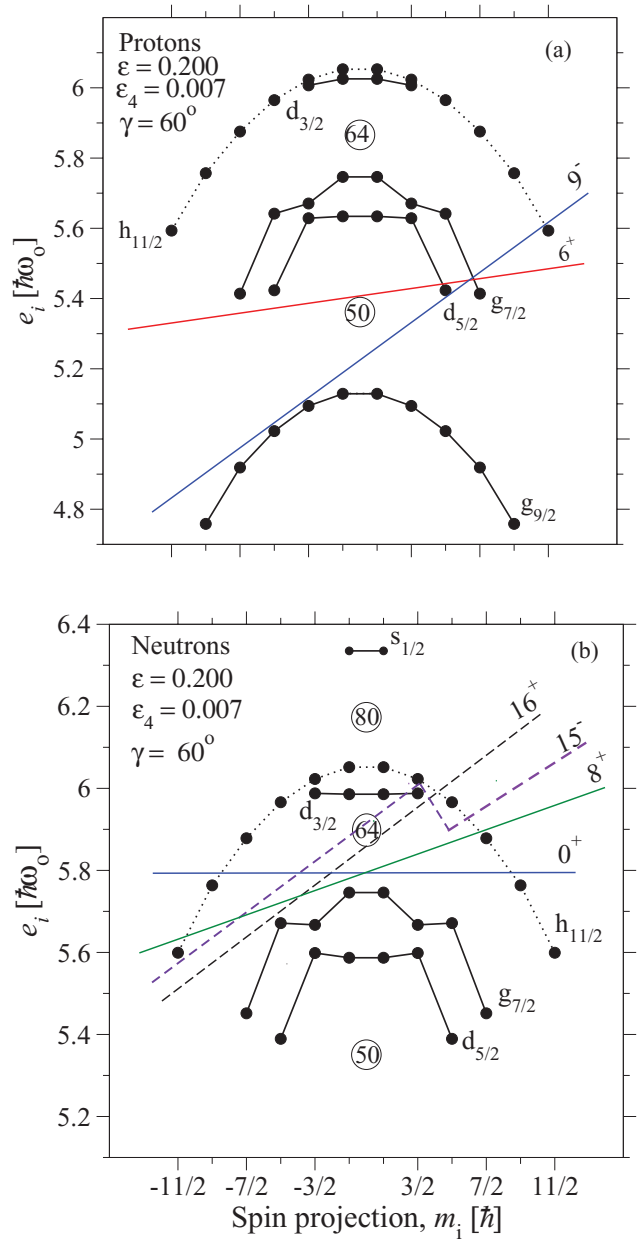

FIG. 7. (Color online) Single-particle energies as a function of the spin projection quantum number for protons (a) and neutrons (b). Note that the full mixing is included in the calculations; i.e., the j-shell labels are only approximations. Straight-line Fermi surfaces are drawn to indicate favored aligned states.

for neutrons, and

$$\pi(g_{7/2}, d_{5/2})^2; I^\pi_{\rm max} = 6^+, \quad \pi(g_{7/2}, h_{11/2}); I^\pi_{\rm max} = 9^-$$

for protons. Note that the total number of particles and not only the aligned particles in the j shells are listed. With two aligned $h_{11/2}$ neutrons, $I^\pi_{\rm max} = 8^+$ (listed in brackets) is obtained in our unpaired calculations (see Fig. 7) while calculations with pairing give $I^\pi_{\rm max} = 10^+$. Fully aligned terminating states may be obtained by combining these neutron and proton excitations to states with $I^\pi = (14^+), 16^+, (17^-), 19^-, 21^-, 22^+, 24^+$, and 25^-, respectively. The terminating states obtained in

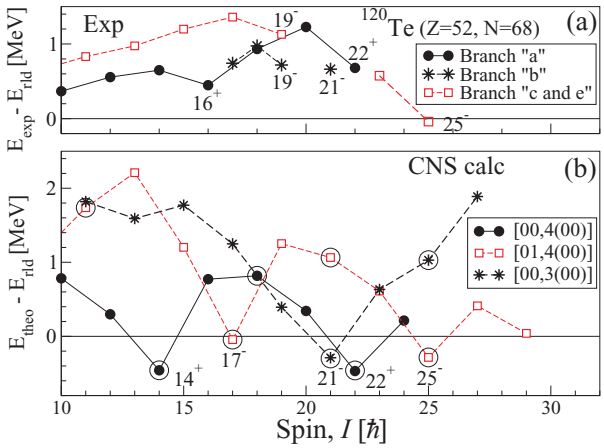

FIG. 8. (Color online) Excitation energies, relative to a rotating liquid-drop energy, for observed (a) and calculated (b) medium-spin sequences in ^{120}Te. Fully aligned terminating states are encircled.

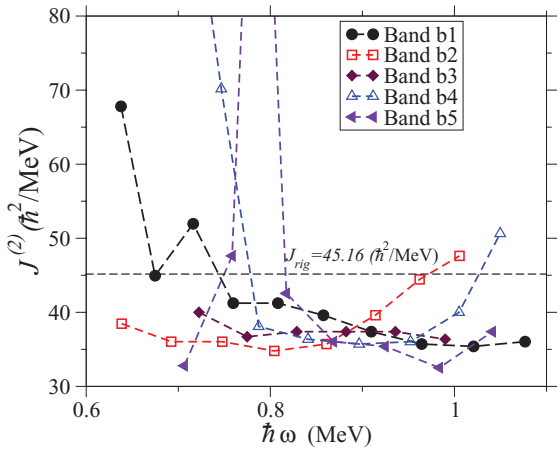

FIG. 9. (Color online) Dynamic moments of inertia, $J^{(2)}$, as a function of rotational frequency for the five new high-spin bands in ^{120}Te.

the calculations without pairing are given in brackets. The observed levels at 5343 (16^+), 7279 (19^-), 7762 (21^-), 8289 (22^+), and 9217 (25^-) keV (see level scheme in Fig. 1) may be interpreted in this way. Note that the maximum spin that can be generated within the valence space is $I = 25$.

The experimental and calculated excitation energies relative to a rotating liquid drop for different level sequences are plotted as a function of spin in Fig. 8. The calculated aligned states are encircled with the spin values written for those cases which are represented by straight-line Fermi surfaces in Fig. 7. These terminating states are associated with an oblate deformation with shape parameters $\varepsilon_2 \simeq 0.18$ and $\gamma = 60^\circ$.

The first level that appears to be favored in energy is the $I^\pi = 16^+$ state of structure a (see upper panel of Fig. 8). Analogous states have been observed in the neighboring Te isotopes, ^{116}Te [6] and ^{118}Te [7]. The configuration of the 16^+ state is obtained by coupling the fully-aligned proton configuration with $I^\pi_{\max} = 6^+$ to a pair of aligned $h_{11/2}$ neutrons; i.e., $\pi(g_{7/2}, d_{5/2})^2_6 \otimes \nu(h^2_{11/2})_{10}$. As mentioned above, the CNS calculation gives a favored state with $I^\pi = 14^+$ for this configuration due to one anti-aligned neutron; i.e., $\pi(g_{7/2}, d_{5/2})^2_6 \otimes \nu(h^2_{11/2})_0(h^2_{11/2})_8$ or [00,4(00)], see Figs. 7 and 8. The highest-spin state of sequence a, the 22^+ level, is obtained by coupling the aligned 6^+ proton configuration to neutron states with another broken pair in the $h_{11/2}$ orbitals; i.e., $(h_{11/2})^4_{16}$.

Structures c and e have negative parity, where e is the continuation of c to higher spins. The presence of negative-parity sequences at low energy is a common feature in neutron-deficient even-even Te nuclei [6,7]. For the configuration of the analogous band in ^{116}Te, the two-quasi-neutron configuration $\nu(h_{11/2}d_{3/2})$ was suggested, whereas in ^{118}Te the $\pi(h_{11/2}g_{7/2})$ configuration was assigned to the respective bands. According to the present CNS calculation, an excitation of one proton from the mixed $g_{7/2}d_{5/2}$ into $h_{11/2}$ orbitals with two unpaired $h_{11/2}$ neutrons may explain the negative-parity states of sequence c; i.e., the configuration [01,4(00)] corresponding to $\pi[(g_{7/2}d_{5/2})h_{11/2}]_9 \otimes \nu[(h^2_{11/2})_0(h^2_{11/2})]_8$ for the terminating state, with the two $h_{11/2}$ neutrons coupled to $I^\pi_{\max} = 8^+$ in the calculations without pairing. Similar to sequence a (see above), these calculations predict a favored state with $I^\pi = 17^-$, while experimentally the $I^\pi = 19^-$ level is found to be low in energy.

The configuration [00,3(00)] is favored by the CNS calculations in the spin region between 19 and 21. The calculated relative excitation energies are included in the lower panel of Fig. 8. The maximally aligned state of this configuration; i.e., $\pi[(g_{7/2}, d_{5/2})^2]_6 \otimes \nu[(h_{11/2})^3(d_{3/2})]_{15}$, is assigned to the observed 21^- level at 7762 keV. The [01,4(00)] configuration becomes again yrast above $I^\pi = 23^-$ and continues up to a maximally aligned state within the valence space; i.e., $\pi[(g_{7/2}, d_{5/2})h_{11/2}]_9 \otimes \nu[(h_{11/2})^4]_{16}$ with $I^\pi = 25^-$. Therefore, it is assigned to branch e, with the 25^- level as the fully aligned state.

Sequence f is placed on top of the 22^+ state in the level scheme. Higher-spin states, beyond the valence space with $I_{\max} = 25$, can be created by a hole in the $N = 64$ core where the particle may occupy either $h_{11/2}$ or $d_{3/2}s_{1/2}$ orbitals. This would lead to configurations like, e.g., [01,5(00)].

B. High-spin bands

The dynamic moments of inertia, $J^{(2)}$, of the five high-spin bands are presented as a function of rotational frequency in Fig. 9. The $J^{(2)}$ values are quite similar, but they are clearly smaller than the rigid body value at a typical ground state deformation, $1/2J_{\text{rig}} \approx 32.32A^{-5/3}\text{MeV}/\hbar^2$ [17], which is also given in the figure. The prominent spike for b5 at $\hbar\omega = 0.79$ MeV may be explained by an alignment of a pair of $h_{11/2}$ neutrons. A similar alignment was observed in neighboring ^{118}Te; however, at a lower frequency of $\hbar\omega = 0.6$ MeV [7].

At the highest observed frequencies, a sudden increase in $J^{(2)}$ is seen for b4 and, to a lesser extent, for b5, analogous to those observed in high-spin bands of ^{126}Xe [20]. For the bands in ^{120}Te, this increase of $J^{(2)}$ is probably caused by irregularities close to termination for the associated configurations (see below).

Bands with similar properties as b1 to b5 have been observed recently in ^{125}I [18], ^{125}Xe [19], ^{126}Xe [20], and

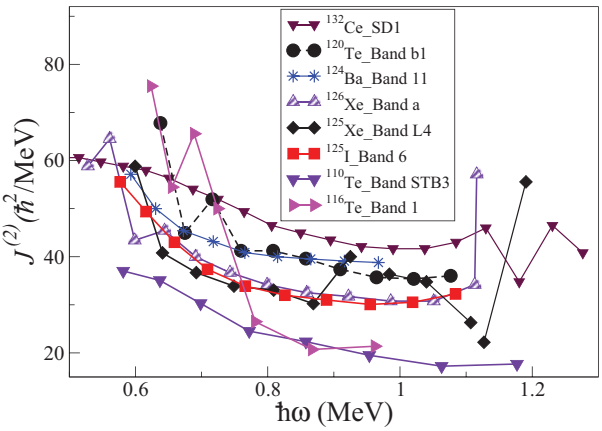

FIG. 10. (Color online) Dynamic moments of inertia, $\mathcal{J}^{(2)}$, as a function of rotational frequency for the high-spin band b1 in ^{120}Te as well as for similar bands in this mass region. For comparison, the SD band in ^{132}Ce and the smooth terminating bands in ^{110}Te and ^{116}Te are included.

^{124}Ba [21]. The dynamic moments of inertia of several of these bands are compared to those of band b1 in Fig. 10. For comparison, the yrast SD band in ^{132}Ce [40] and the smooth terminating bands in ^{110}Te [41] and ^{116}Te [6] are included, where the latter is, however, smooth only in a short frequency range.

The moments of inertia of the bands in ^{120}Te are similar to those of the bands in the $A \simeq 125$ region, but they are larger than those in the $A \simeq 110$ region. In both mass regions the high-spin bands are characterized by proton holes in the $g_{9/2}$ subshell below the $Z = 50$ gap. On the other hand, the neutrons in open shells are essentially limited to the $g_{7/2}d_{5/2}$ and $h_{11/2}$ subshells in the $A \simeq 110$ region while they explore all the subshells in the $N = 50$–82 shell in the $A = 125$ region, with an additional possibility to excite neutrons across the $N = 82$ gap. The bands in ^{120}Te probably have similar configurations as the previously observed bands in the $A = 125$ region; however, most likely without particle excitations across the $N = 82$ gap (see below).

Satisfactory agreement between experimental properties and results of CNS calculations was not generally achieved in the previous work [18,21]. This is surprising, considering the successful description of high-spin bands within the CNS approach in other mass regions. Therefore, it is interesting to test if the CNS model would work well in the present case of ^{120}Te.

In order to describe all low-energy configurations in the $I = 30 - 50$ spin range, excitations across the $Z = 50$ shell gap for protons as well as excitations within the $N = 50 - 82$ valence space and across the $N = 82$ shell gap for neutrons were taken into account. In the calculations, all combinations of parity and signature [$\pi = (+, -), \alpha = (0, 1)$] were considered. Calculated energies relative to a rotating liquid drop for configurations that could describe the data are summarized in Fig. 11. The calculated bands correspond to a prolate or close-to-prolate shape in the $I = 30 - 40$ spin range. As seen in the figure, they are yrast or close to yrast at these spin values, but compete with less collective configurations at γ

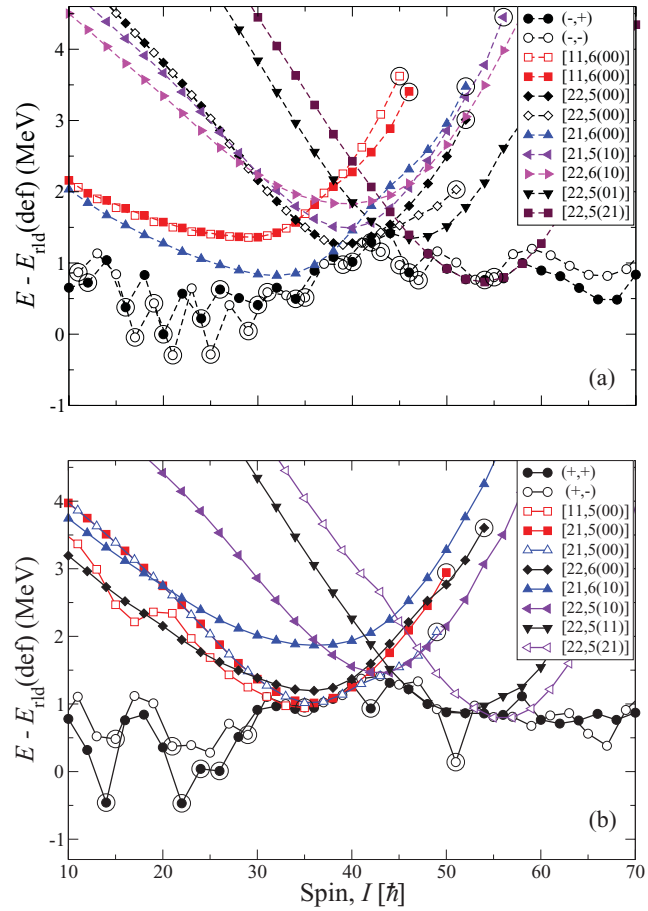

FIG. 11. (Color online) Calculated excitation energies relative to a rotating liquid-drop energy as a function of spin for the lowest-energy configurations for ^{120}Te. (a) Negative-parity; (b) positive-parity configurations. For some configurations the two signatures are plotted separately. For comparison, the calculated yrast lines for both signatures and parities are included. Fully aligned terminating states are encircled.

values close to the noncollective limit, $\gamma = 60^\circ$. Indeed, the irregularities at high spin in some of the curves are caused by local minima with $\gamma \simeq 40^\circ$ which, in some cases, are lower in energy than the minima with $\gamma \simeq 0^\circ$.

Single-particle Routhians for protons and neutrons at a prolate deformation are given in Fig. 12. They are helpful to understand the single-particle occupancy of orbitals for the calculated bands. In the case of protons, the $g_{9/2}$ orbital with $\Omega = 9/2$ crosses the $g_{7/2}d_{5/2}$ level with $\Omega = 3/2$, which dives down below the Fermi level at a frequency of $\hbar\omega \simeq 0.5$ MeV. In the frequency range of $\hbar\omega \simeq 0.6$–1.0 MeV, corresponding to the collective bands in ^{120}Te, configurations with two $g_{9/2}$ holes and one or two $h_{11/2}$ protons are favored. The favored neutron configurations have five or six particles in the $h_{11/2}$ subshell. In addition, it is important to consider how many neutrons are excited across the spherical $N = 64$ gap from the orbitals of $g_{7/2}d_{5/2}$ to orbitals of $d_{3/2}s_{1/2}$ character. However, these orbitals are strongly mixed and it is not possible to fix configurations according to the number of $g_{7/2}d_{5/2}$ and $d_{3/2}s_{1/2}$ neutrons, respectively. Instead, only the

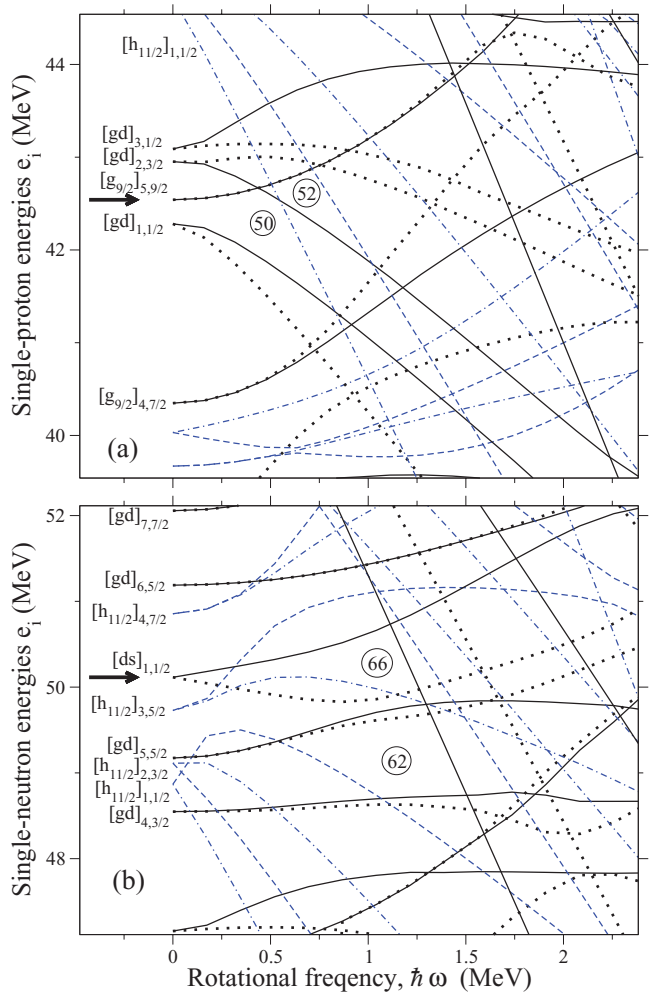

FIG. 12. (Color online) Single-particle proton (a) and neutron (b) energies in a rotating frame as a function of rotational frequency at a fixed deformation of $\varepsilon_2 = 0.23$, $\varepsilon_4 = 0.04$, and $\gamma = 1^\circ$. The four combinations of (π, α) are displayed in the following way: solid lines represent $(+, 0)$ and dotted lines indicate $(+, 1)$, whereas $(-, 0)$ and $(-, 1)$ are represented by dashed and dashed-dotted lines, respectively. The orbitals are labeled for zero rotational frequency. Orbitals with their main amplitudes in the $g_{7/2}d_{5/2}$ and $d_{3/2}s_{1/2}$ subshells are labeled as [gd] and [ds], respectively, with the ordering and angular momentum projection Ω as subscripts. The two arrows indicate the position of the Fermi level.

total number of orbitals in these subshells, labeled as 'gd' and 'ds', respectively, in the following, can be specified. Some irregularities in the bands are caused by excitations within these $N = 4$ neutron subshells. However, for the bands which terminate, it is straightforward to specify the number of particles excited across the $N = 64$ gap in the terminating states (see below). At the deformation used in Fig. 12, the orbitals emerging from the $i_{13/2}$ and $h_{9/2}f_{7/2}$ subshells above the $N = 82$ gap become energetically competitive only around $\hbar\omega = 1.1$–1.2 MeV. This suggests that they are not active in the observed high-spin bands of ^{120}Te (see also below).

In order to generate collective bands, it is necessary to excite at least one proton across the $Z = 50$ gap. However, with only one excited proton, the bands do either terminate too low in spin; e.g., at $I = 36$ for the even-spin sequence of the [11,5(00)] configuration, or too high in energy as, e.g., for the $I = 45, 46$ terminating states of the [11,6(00)] configuration (see Fig. 11). These spin values are so different because the former configuration terminates with one hole in the spherical $N = 64$ core; i.e., in the neutron configuration $\nu[(gd)^{-1}_{5/2}(h_{11/2})^5_{35/2}]_{20}$, while the latter configuration terminates with four such holes; i.e., in the $\nu[(gd)^{-4}_{10}(h_{11/2})^6_{18}](ds)^2_2]_{30}$ configuration. The proton configuration is the same in both instances, $\pi[(g_{9/2})^{-1}_{7/2,9/2}(gd)^2_6 (h_{11/2})^1_{11/2}]_{15,16}$.

The configurations which give the best description of the observed bands are those with two $g_{9/2}$ proton holes. Negative-parity bands of this kind terminate at $I^\pi = 52^-$ (see Fig. 11) in either the [21,6(00)] configuration; i.e.,

$$\pi\left[(g_{9/2})^{-2}_8(gd)^3_{17/2}h_{11/2}\right]_{22} \otimes \nu\left[(gd)^{-4}_{10}(h_{11/2})^6_{18}(ds)^2_2\right]_{30}$$

or in the [22,5(00)] configuration; i.e.,

$$\pi\left[(g_{9/2})^{-2}_8(gd)^2_6(h_{11/2})^2_{10}\right]_{24} \otimes \nu\left[(gd)^{-3}_{17/2}(h_{11/2})^5_{35/2}(ds)^2_2\right]_{28}.$$

If these proton and neutron configurations are combined in different ways, the positive-parity configurations [21,5(00)] or [22,6(00)] are formed, which terminate (see Fig. 11) at $I^\pi = 50^+$ and 54^+, respectively.

Configurations with a higher spin content can be formed with one neutron excited across the $N = 82$ gap to the $h_{9/2}$, $f_{7/2}$, or $i_{13/2}$ orbitals. These are the strongly down-sloping orbitals which come down to the Fermi surface for frequencies $\hbar\omega \approx 1$ MeV in Fig. 12. However, it appears that they should not be assigned to the observed collective bands. As seen in Fig. 11, with one $h_{11/2}$ proton as in the [21,5(10)] or [21,6(10)] configurations, they are calculated too high in energy while with two $h_{11/2}$ protons as in the [22,5(10)] or [22,6(10)] configurations, they have their energy minima too high in spin. Furthermore, in the low-spin range of the observed collective bands, around $I = 30$, they are calculated to lie high above yrast and, thus, provide no satisfactory description of the data.

1. Band b1

The experimental excitation energies of bands b1 to b5 relative to a rotating liquid drop energy are plotted as a function of spin in the upper panel of Fig. 13. Note that excitation energies and spins of b2 to b5 are estimates based on their decay patterns. The results of the CNS calculations for the most favored configurations (as argued above) are presented in the middle panel of the figure, and the differences between calculated and experimental energies are shown in the lower panel.

For negative parity, the [21,6(00)] configuration is the lowest up to $I^\pi = 38^-$; but, at higher spins, the [22,5(00)] structure is calculated to lie lower in energy. Since negative parity is only tentatively assigned to b1, positive-parity configurations might be considered as well. The positive-parity configurations [22,6(00)] and [21,5(00)] lie about equally low in energy. For all configurations the difference between calculations and experiment falls in the range of 1–2 MeV

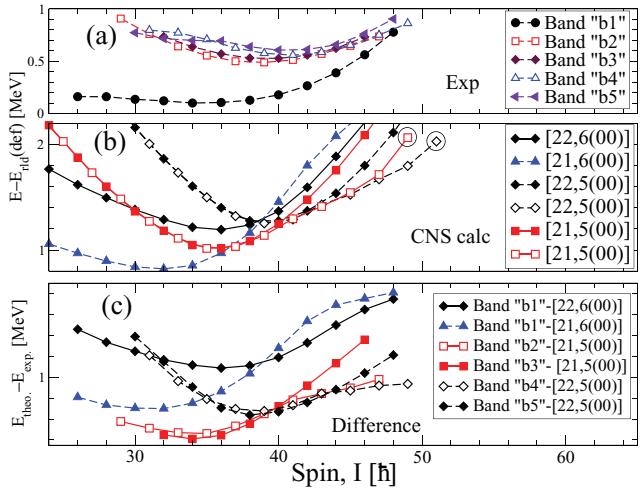

FIG. 13. (Color online) Excitation energies relative to a rotating liquid-drop energy for the observed bands b1 to b5 in ^{120}Te (a) and for calculated (b) configurations. The differences between the observed and calculated energies can be found in (c). Note that experimental energies for b2 to b5 are estimated.

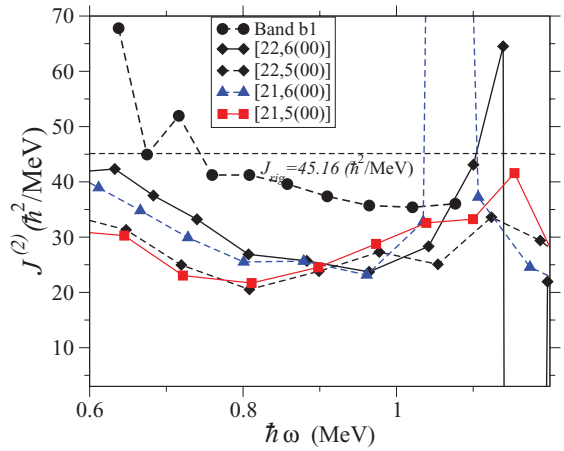

FIG. 14. (Color online) Calculated dynamic moments of inertia, $J^{(2)}$, as a function of rotational frequency for several configurations and experimental values of b1. The dashed line represents the rigid-body moment of inertia for $A = 120$.

for most spin values. Such deviations may still be acceptable since typical differences between calculations and experiment lie around 1 MeV [31], and even larger differences can be expected in some instances. However, the shape of the difference curves is more relevant. The energy differences are expected to become constant at high spins, and to increase with decreasing spin, where pairing correlations are important. The two negative-parity configurations, which are the favored candidates for the structure of b1, show rather different features. The difference curve for the [21,6(00)] configuration exhibits a strange S-shape and that for the [22,5(00)] configuration (not shown for b1 in Fig. 13 since it is tentatively assigned to the signature-partner bands b4/b5, see below) increases too fast with decreasing spin. For the two configurations with positive parity, [22,6(00)] and [21,5(00)] (not shown for b1 in Fig. 13 since it is tentatively assigned to the signature-partner bands b2/b3, see below), the increase in the high-spin range is problematic.

To further test the suggested configuration assignments, the experimental dynamic moments of inertia, $J^{(2)}$, of band b1 are compared in Fig. 14 with the calculations for the four configurations discussed above. The calculated values are similar; however, they are significantly smaller than the experimental moments of inertia. The favorite negative-parity configuration, [21,6(00)], shows a pronounced alignment at $\simeq 1.1$ MeV which is absent in the data. With pairing included, the calculated energies would probably come down at low spins leading to a smaller curvature and, thus, to larger $J^{(2)}$ values, but this can probably only explain part of the differences between calculations and experiment.

Even though it seems difficult to assign the exact configuration for band b1, configurations with two $g_{9/2}$ proton holes, one or two $h_{11/2}$ protons and five or six $h_{11/2}$ neutrons are most likely. Furthermore, according to the CNS calculations, these configurations have at most four holes in the $g_{7/2}$ and $d_{5/2}$ subshells below the spherical $N = 64$ gap (the $[gd]_6$ and $[gd]_7$ orbitals in Fig. 12 corresponding to the [402]5/2 and [404]7/2 orbitals at a prolate shape). As discussed above, these configurations terminate at $I_{\max} = 50$ to 54.

Total energy surfaces for the [21,6(00)] configuration are displayed in Fig. 15. At spins around $I = 30$–40, a stable prolate minimum at $\varepsilon_2 \simeq 0.23$ is calculated. This deformation is smaller than those derived from DSAM lifetime measurements for high-spin bands in ^{125}Xe [19] and ^{126}Xe [20], where $\varepsilon_2 = 0.26 - 0.34$ was estimated. At the highest spins for the [21,6(00)] configuration, the deformation decreases rapidly; for $I^\pi = 46^-$, $\varepsilon_2 \approx 0.15$ is calculated and, finally, the band terminates at $I^\pi = 52^-$ with close to spherical shape.

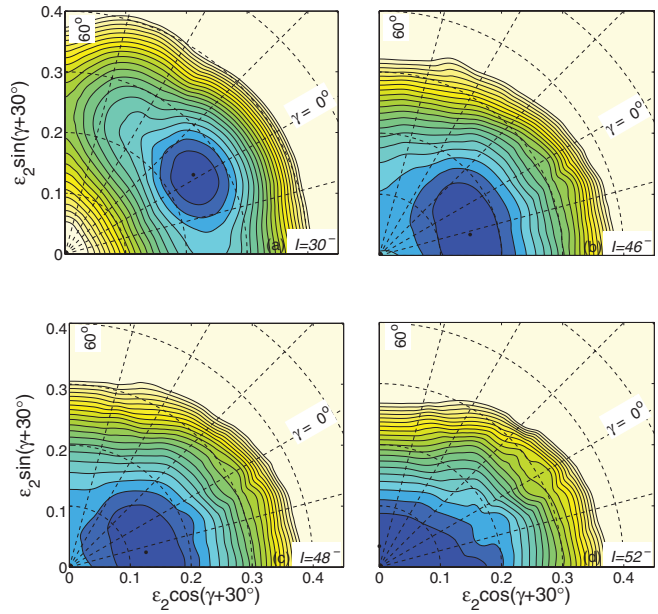

FIG. 15. (Color online) Calculated total energy surfaces for the [21,6(00)] configuration showing the near-spherical termination at the highest spins. The contour-line separation is 0.25 MeV.

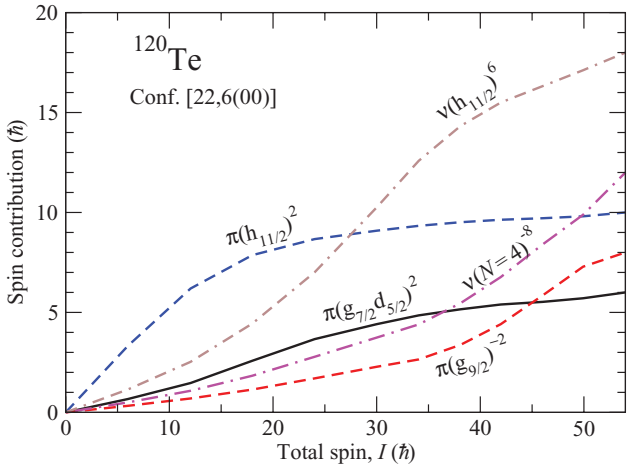

FIG. 16. (Color online) Calculated contributions to the angular momentum of the [22,6(00)] configuration of ^{120}Te shown as a function of spin. The calculations were carried out along the shape trajectory of this configuration.

It is interesting to compare this behavior with the smooth terminating bands in the $A = 110$ region [17] where the termination occurs at an oblate shape with $\varepsilon_2 = 0.10$–0.15. The reason for the difference is that in the $A = 110$ region the bands are dominated by particles with only two holes in the $g_{9/2}$ proton subshell. The present bands in ^{120}Te, on the other hand, have a larger number of holes in the associated core. Relative to a ^{114}Sn core, they have four neutron holes in the $g_{7/2}$ and $d_{5/2}$ subshells in addition to two $g_{9/2}$ proton holes. A consequence of the similar number of holes and particles is that the bands in ^{120}Te terminate at a much higher excitation energy, making it difficult to observe these bands up to their termination.

The similarities and differences between the present bands in ^{120}Te and the smooth terminating bands in the $A = 110$ region is also reflected in the way the angular momentum is generated. This is illustrated for the [22,6(00)] configuration of ^{120}Te in Fig. 16 and may be compared with a corresponding figure for the [21,4(00)] configuration of ^{110}Sb (see Fig. 31 of Ref. [17]). The particles in high-j shells align at low rotational frequencies, as seen for the $h_{11/2}$ protons. The four $h_{11/2}$ neutrons in ^{110}Sb are also relatively easy to align, while it is somewhat more difficult to align the six $h_{11/2}$ neutrons in ^{120}Te. The two $g_{9/2}$ proton holes align only at high rotational frequencies. In addition, there are $N = 4$ neutrons in ^{120}Te which are dominated by four holes in the gd orbitals. Therefore, they show a behavior similar to that of the $g_{9/2}$ holes. This is rather different from the $N = 4$ neutrons in ^{110}Sb which are described as six particles in the gd orbitals. These subshells are close to half-filled and still relatively easy to align.

2. *Bands b2 to b5*

The spins and parities of the bands b2 to b5 are not firmly determined. Therefore, it is even more challenging to propose configuration assignments for these bands. With the most likely choice of spins and excitation energies, bands b2 and b3 and bands b4 and b5 become signature degenerate in most of the observed spin range, see Fig. 13, upper panel. Considering the single-particle Routhians displayed in Fig. 12, signature-degenerate bands may be formed either with one proton in the highest $g_{9/2}$ proton orbital or with one neutron in the $[gd]_6$ orbital; i.e., the [402]5/2 state at a prolate shape. The former case corresponds to $(g_{9/2})^{-1}$ and it was already concluded above that, mainly because of their low spin content, these configurations cannot describe the smooth collective bands which are observed up to spin values close to $I = 50$. This suggests that the bands are formed with one neutron in the $[gd]_6$ orbital and five $h_{11/2}$ neutrons for $N = 68$. The two low-lying $\pi(g_{9/2})^{-2}$ configurations of this kind, [21,5(00)] and [22,5(00)], are both drawn in Fig. 13. In the lower panel of the figure, it is assumed that bands b2 and b3 have the [21,5(00)] and bands b4 and b5 the [22,5(00)] configuration. The differences between experiment and calculations are found within 0.5 MeV of those for band b1. Thus, there are clearly also some difficulties with this interpretation. For example, the calculated energy for the [22,5(00)] configuration increases too fast with decreasing spin, leading to large values for the energy differences. Furthermore, the signature degeneracy is reproduced by the calculations up to $I \approx 40$ but, for higher spin values, the calculated bands start to split up when the deformation becomes smaller.

The suggested assignments for bands b2 to b5 are certainly tentative and should be taken as an illustration that it is possible to find some correspondence between calculations and experiment. An important input is that the bands are assumed to be signature partners which is reasonable but still uncertain. With the assumption of signature degeneracy, it might still be possible to change the spins of one or the other band by $1\hbar$ or to change the assignment; i.e., that bands b2 and b3 are assigned to the [22,5(00)] and bands b4 and b5 to the [21,5(00)] configuration.

V. SUMMARY

High-spin states in ^{120}Te were investigated using the Gammasphere spectrometer. The medium-spin level scheme was extended up to several fully-aligned states within the valence space. At higher spins, five collective bands, extending up to $I \approx 50$, were discovered. However, only one of these bands could be linked to lower-lying levels.

The structure of the noncollective and collective states was investigated within the framework of the CNS model. Configuration assignments were proposed for the near-spherical structures and for the fully aligned states. However, an unambiguous description of the collective high-spin bands was not possible. A configuration with two protons excited from the $g_{9/2}$ orbital and six neutrons in the $h_{11/2}$ subshell is suggested for the connected band b1. The bands b2 to b5 are tentatively arranged in two signature-partner pairs and configurations with two $g_{9/2}$ proton holes and five $h_{11/2}$ neutrons are suggested. With this interpretation, all the bands are observed up to close to their terminating spin values. However, the differences in energy between experiment and calculation are rather large, as was previously also observed for similar bands in nuclei of

this mass region. This discrepancy should be further explored theoretically.

ACKNOWLEDGMENTS

The authors are grateful to G. B. Hagemann for valuable comments on this work. S.N. acknowledges financial support from CSIR, India, under Contract No. 09/081(0704)/2009-EMR-I and is grateful for help received from Purnima Singh. The authors thank the ANL ATLAS and Gammasphere operations staff. This work was supported by DST, India, under Contract No. SR/S2/HEP-09/2005, by the Swedish Natural Science Research Council, by the German BMBF under Contract No. 06 BN 109, by the Danish FNU Council for Natural Sciences, by the U.S. Department of Energy, Office of Nuclear Physics, under Contracts No. DE-AC02-06CH11357 and No. DE-AC03-76SF00098, by OTKA, Hungary, under Contract No. K72566, and by the New Hungary Development Plan under Contract No. TÁMOP4.2.1./B-09/1/KONV-2010-0007/IK/IT.

[1] J. L. Wood, K. Heyde, W. Nazarewicz, M. Huyse, and P. Van Duppen, Phys. Rep. **215**, 101 (1992).
[2] R. Wadsworth *et al.*, Phys. Rev. C **50**, 483 (1994).
[3] H. Schnare *et al.*, Phys. Rev. C **54**, 1598 (1996).
[4] A. K. Gaigalas, R. E. Shroy, G. Schatz, and D. B. Fossan, Phys. Rev. Lett. **35**, 555 (1975).
[5] R. E. Shroy, A. K. Gaigalas, G. Schatz, and D. B. Fossan, Phys. Rev. C **19**, 1324 (1979).
[6] J. M. Sears *et al.*, Phys. Rev. C **55**, 2290 (1997).
[7] S. Juutinen *et al.*, Phys. Rev. C **61**, 014312 (1999).
[8] E. S. Paul, D. B. Fossan, J. M. Sears, and I. Thorslund, Phys. Rev. C **52**, 2984 (1995).
[9] Y. Liang, R. Ma, E. S. Paul, N. Xu, D. B. Fossan, J.-y. Zhang, and F. Dönau, Phys. Rev. Lett. **64**, 29 (1990).
[10] C.-B. Moon and T. Komatsubara, J. Korean Phys. Soc. **45**, L791 (2004).
[11] A. K. Singh *et al.*, Phys. Rev. C **70**, 034315 (2004).
[12] E. S. Paul, D. B. Fossan, G. J. Lane, J. M. Sears, I. Thorslund, and P. Vaska, Phys. Rev. C **53**, 1562 (1996).
[13] V. P. Janzen *et al.*, Phys. Rev. Lett. **72**, 1160 (1994).
[14] D. R. LaFosse *et al.*, Phys. Rev. C **50**, 1819 (1994).
[15] I. Thorslund *et al.*, Phys. Rev. C **52**, R2839 (1995).
[16] I. Ragnarsson, V. P. Janzen, D. B. Fossan, N. C. Schmeing, and R. Wadsworth, Phys. Rev. Lett. **74**, 3935 (1995).
[17] A. V. Afanasjev, D. B. Fossan, G. J. Lane, and I. Ragnarsson, Phys. Rep. **322**, 1 (1999).
[18] Purnima Singh *et al.*, Phys. Rev. C **84**, 024316 (2011).
[19] A. Al-Khatib *et al.*, Phys. Rev. C **83**, 024306 (2011).
[20] C. Rønn Hansen *et al.*, Phys. Rev. C **76**, 034311 (2007).
[21] A. Al-Khatib *et al.*, Phys. Rev. C **74**, 014305 (2006).
[22] R. M. Clark *et al.*, Phys. Rev. Lett. **76**, 3510 (1996).
[23] E. S. Paul *et al.*, Phys. Rev. C **71**, 054309 (2005).
[24] I. Y. Lee *et al.*, Nucl. Phys. A **520**, 641c (1990).
[25] D. C. Radford, Nucl. Instrum. Methods Phys. Res. A **361**, 297 (1995).
[26] J. J. Van Ruyven *et al.*, Nucl. Phys. A **380**, 125 (1982).
[27] P. Chowdhury, W. F. Piel, and D. B. Fossan, Phys. Rev. C **25**, 813 (1982).
[28] T. Bengtsson and I. Ragnarsson, Nucl. Phys. A **436**, 14 (1985).
[29] I. Ragnarsson, Phys. Lett. B **264**, 5 (1991).
[30] A. V. Afanasjev and I. Ragnarsson, Nucl. Phys. A **608**, 176 (1996).
[31] B. G. Carlsson and I. Ragnarsson, Phys. Rev. C **74**, 011302(R) (2006).
[32] Purnima Singh *et al.*, Phys. Rev. C **82**, 034301 (2010).
[33] K. Starosta *et al.*, Phys. Rev. C **64**, 014304 (2001).
[34] D. Glas, U. Mosel, and P. G. Zint, Z. Phys. A **285**, 83 (1978).
[35] J.-y. Zhang, N. Xu, D. B. Fossan, Y. Liang, R. Ma, and E. S. Paul, Phys. Rev. C **39**, 714 (1989).
[36] K. Pomorski and J. Dudek, Phys. Rev. C **67**, 044316 (2003).
[37] S. G. Rohozinski, Phys. Rev. C **56**, 165 (1997).
[38] G. Andersson *et al.*, Nucl. Phys. A **268**, 205 (1976).
[39] M. J. A. DeVoigt, J. Dudek, and Z. Szymanski, Rev. Mod. Phys. **55**, 949 (1983).
[40] E. S. Paul *et al.*, Phys. Rev. C **71**, 054309 (2005).
[41] E. S. Paul *et al.*, Phys. Rev. C **76**, 034323 (2007).